

Variational quantum-neural hybrid imaginary time evolution

Hiroki Kuji,* Tetsuro Nikuni, and Yuta Shingu†
*Department of Physics, Tokyo University of Science,
1-3 Kagurazaka, Shinjuku, Tokyo, 162-8601, Japan*
(Dated: March 31, 2025)

Numerous methodologies have been proposed for performing imaginary time evolution (ITE) using quantum computers. Among these, variational ITE (VITE) for noisy intermediate-scale quantum (NISQ) computers has attracted much attention, which uses parametrized quantum circuits to mimic non-unitary dynamics. However, conventional variational quantum algorithms including VITE face challenges in achieving high accuracy due to their strong dependence on the choice of ansatz quantum circuits. Recently, the variational quantum-neural eigensolver (VQNHE), which combines the neural network (NN) with the variational quantum eigensolver, has been proposed. This approach enhances performance of estimating the expectation values of the state given by the parametrized quantum circuit and NN. In this study, we propose a variational quantum-neural hybrid ITE method (VQNHITE). Our proposal accurately estimates ITE by combining the NN and parameterized quantum circuit. We tested our approach with numerical simulations to evaluate the performance of VQNHITE relative to VITE.

I. INTRODUCTION

Imaginary time evolution (ITE) is the dynamics obtained by replacing the real-time parameter t with $t \rightarrow -i\beta$ using a real parameter β in the Schrödinger equation. The time evolution operator is written as $e^{-\hat{H}\beta}$, where \hat{H} is the Hamiltonian. ITE is a powerful method and gives rise to numerous applications such as ground state search [1, 2] and the preparation of thermal equilibrium states [3]. For instance, in condensed matter physics, high-energy physics, and quantum chemistry, it is often crucial to determine the ground state [4–12]. However, the ITE operator is nonunitary and cannot be implemented directly on quantum devices. To overcome this limitation, various methods have been proposed to approximate the ITE with quantum computers, such as variational ITE (VITE) [3, 13, 14], quantum ITE [15–18], and probabilistic ITE [1, 19]. Among them, the VITE is implemented on a noisy intermediate-scale quantum (NISQ) computer [20]. The VITE uses a parameterized quantum circuit $\hat{U}(\theta)$ and the circuit parameters θ are iteratively updated by a hybrid process of quantum and classical calculations. However, the accuracy of VITE depends critically on the choice of the ansatz circuit.

Another known application of NISQ devices is the variational quantum eigensolver (VQE) [6, 21–28], which estimates the ground-state energy with $\hat{U}(\theta)$. This approach has the same limitation as VITE. As a promising approach to suppress the problem, a method called variational quantum-neural hybrid eigensolver (VQNHE) [29], which combines the neural network (NN) and quantum circuit, was proposed. In this method, the nonunitary operator $\hat{f}(\phi)$ generated by the NN is used to achieve a much higher expressivity for quantum states. Indeed,

previous studies have also proposed combining classical neural networks with quantum computing techniques to improve the accuracy of the ground-state energy estimation [30–41].

In our study, we propose and investigate the Variational Quantum-Neural Hybrid ITE (VQNHITE) approach, aiming to boost the accuracy of imaginary time evolution (ITE) simulations by combining a parameterized quantum circuit with a classical neural network. Specifically, we prepare the trial quantum state $|\varphi(\theta, \phi)\rangle = \hat{f}(\phi)\hat{U}(\theta)|\bar{0}\rangle$, where $|\bar{0}\rangle$ is an initial state, $\hat{U}(\theta)$ is a parametrized unitary operator, and $\hat{f}(\phi)$ is a nonunitary operator determined by the neural network. Compared to the standard VITE, our hybrid scheme provides greater expressivity, thereby achieving more precise ITE. A key implementation detail lies in how we address the variability arising from the neural network's initial parameters. Rather than relying on arbitrary or randomly chosen initial conditions, we employ a gradient method to determine the initial parameters for the NN and the parameterized unitary operator. We conducted numerical simulations to verify that VQNHITE outperforms the conventional VITE in simulating ITE. Specifically, we computed and plotted the fidelity between each state produced by VQNHITE or VITE and the corresponding state obtained via exact imaginary time evolution. Our results confirm that the proposed VQNHITE framework provides a more accurate estimation of ITE than the conventional VITE method.

This paper is organized as follows. In Sec. II, we present an overview of VITE. In Sec. III, we briefly review the VQNHE. In Sec. IV, we introduce our proposed VQNHITE framework, detailing the combination of the variational quantum circuit and NN for ITE. In Sec. V, we show the numerical results verifying the accuracy and efficiency of VQNHITE. Finally, in Sec. VI, we discuss and summarize our main findings.

* 1223518@ed.tus.ac.jp

† shingu.yuta@gmail.com

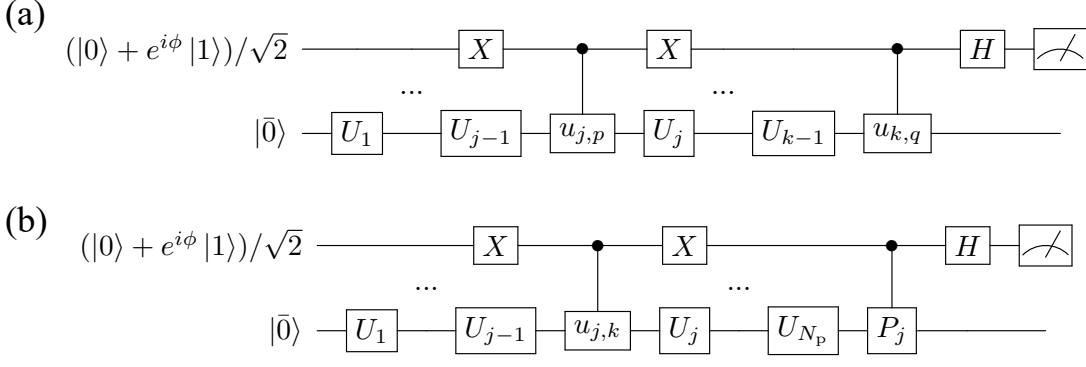


FIG. 1: Quantum circuits for calculating (a) $\text{Re}(e^{i\phi} \langle \bar{0} | \hat{U}_{j,p}^\dagger \hat{U}_{k,q} | \bar{0} \rangle)$ and (b) $\text{Re}(e^{i\phi} \langle \bar{0} | \hat{U}_{j,k}^\dagger \hat{P}_j \hat{U} | \bar{0} \rangle)$ in order to obtain $M_{j,k}$ in Eq. (13) and C_j in Eq. (14). The upper horizontal line (the lower line) represents the ancillary qubit (the qubits of the system). We prepare the initial state $(|0\rangle + e^{i\phi} |1\rangle)/\sqrt{2}$. X and H denote the Pauli \hat{X} gate and the Hadamard gate, and U_j ($j = 1, \dots, N_p$) is a parametrized unitary gate constituting the variational circuit. The expectation values of Z -measurement on the ancillary qubit give (a) $\text{Re}(e^{i\phi} \langle \bar{0} | \hat{U}_{j,p}^\dagger \hat{U}_{k,q} | \bar{0} \rangle)$ and (b) $\text{Re}(e^{i\phi} \langle \bar{0} | \hat{U}_{j,k}^\dagger \hat{P}_j \hat{U} | \bar{0} \rangle)$.

II. VARIATIONAL IMAGINARY TIME EVOLUTION

In this section, we provide an overview of the VITE, which is suitable for NISQ devices. The ITE is governed by the Wick-rotated Schrödinger equation [42, 43], which can be expressed as:

$$\frac{d|\psi(\beta)\rangle}{d\beta} = -(\hat{H} - \langle \psi(\beta) | \hat{H} | \psi(\beta) \rangle) |\psi(\beta)\rangle, \quad (1)$$

where the expectation value $\langle \psi(\beta) | \hat{H} | \psi(\beta) \rangle$ ensures that $|\psi(\beta)\rangle$ remains normalized. Accordingly, the state at imaginary time β is given by

$$|\psi(\beta)\rangle = \frac{\exp(-\hat{H}\beta) |\psi(0)\rangle}{\sqrt{\langle \psi(0) | \exp(-2\hat{H}\beta) | \psi(0) \rangle}}, \quad (2)$$

and has unit norm.

Since the imaginary-time operator $\exp(-\hat{H}\beta)$ is not unitary, we cannot directly prepare the state in Eq. (2) with quantum devices. Alternatively, the variational imaginary time simulation algorithm utilizes a parameterized wavefunction $|\varphi(\boldsymbol{\theta}(\beta))\rangle$, implemented by a parameterized quantum circuit:

$$\begin{aligned} |\varphi(\boldsymbol{\theta}(\beta))\rangle &= \hat{U}(\boldsymbol{\theta}(\beta)) |\bar{0}\rangle \\ \hat{U}(\boldsymbol{\theta}(\beta)) &= \hat{U}_{N_p}(\theta_{N_p}) \cdots \hat{U}_2(\theta_2) \hat{U}_1(\theta_1), \end{aligned} \quad (3)$$

where $\hat{U}_i(\theta_i)$ ($i = 1, \dots, N_p$) represents a parameterized gate, N_p is the total number of parameters, θ_i is a real parameter, and $|\bar{0}\rangle$ is the initial state of the ansatz, typically chosen as $|\psi(0)\rangle$.

Next, we lead to an evolution of the parameters from Eq. (1). To derive the equations for $\partial\boldsymbol{\theta}(\beta)/\partial\beta$, we apply

the McLachlan variational principle, which minimizes the distance:

$$\delta \left\| \left(\frac{\partial}{\partial\beta} + \hat{H} - \langle \varphi(\boldsymbol{\theta}(\beta)) | \hat{H} | \varphi(\boldsymbol{\theta}(\beta)) \rangle \right) |\varphi(\boldsymbol{\theta}(\beta))\rangle \right\| = 0, \quad (4)$$

where the expectation value $\langle |\varphi(\boldsymbol{\theta}(\beta))\rangle | \hat{H} | \varphi(\boldsymbol{\theta}(\beta))\rangle$ ensures the trial state $|\varphi(\boldsymbol{\theta}(\beta))\rangle$ is normalized, and $\| |\psi\rangle \| \equiv \langle \psi | \psi \rangle$ represents the norm of $|\psi\rangle$. This leads to

$$M \frac{\partial\boldsymbol{\theta}(\beta)}{\partial\beta} = \mathbf{C}, \quad (5)$$

where

$$M_{j,k} = \text{Re} \left(\frac{\partial \langle \varphi(\boldsymbol{\theta}(\beta)) | \varphi(\boldsymbol{\theta}(\beta)) \rangle}{\partial\theta_j} \frac{\partial \langle \varphi(\boldsymbol{\theta}(\beta)) | \varphi(\boldsymbol{\theta}(\beta)) \rangle}{\partial\theta_k} \right), \quad (6)$$

$$C_j = -\text{Re} \left(\langle \varphi(\boldsymbol{\theta}(\beta)) | \hat{H} \frac{\partial |\varphi(\boldsymbol{\theta}(\beta))\rangle}{\partial\theta_j} \right), \quad (7)$$

where, $\text{Re}(z)$ denotes the real part of z . The matrices M and \mathbf{C} have dimensions determined by the number of parameters N_p rather than the number of qubits. The ITE in Eq. (5) can be approximated by the Euler method with a small step size $\delta\beta$, leading to

$$\boldsymbol{\theta}(\beta + \delta\beta) \simeq \boldsymbol{\theta}(\beta) + M^{-1}(\beta) \cdot \mathbf{C}(\beta) \delta\beta. \quad (8)$$

We now consider the derivative of the parameterized quantum gate. We assume that the derivative of each parameterized gate \hat{U}_j is decomposed as

$$\frac{\partial\hat{U}_j}{\partial\theta_j} = \sum_k a_{j,k} \hat{U}_j \hat{u}_{j,k}, \quad (9)$$

where $\hat{u}_{j,k}$ is a unitary operator and $a_{j,k}$ is a complex coefficient. For example, if we choose $\exp(-i\theta_j\hat{\sigma}^x)$ as $\hat{U}_j(\theta_j)$, the decomposition is written as

$$\frac{d\hat{U}_j}{d\theta_j} = -i\hat{U}_j(\theta_j)\hat{\sigma}^x, \quad (10)$$

which gives $a_{j,k} = -i$, $\hat{u}_{j,k} = \hat{\sigma}^x$, and $\hat{\sigma}^x$ is the Pauli \hat{X} operator. Consequently, the derivative of the parameterized state can be written as

$$\frac{\partial |\varphi(\boldsymbol{\theta}(\beta))\rangle}{\partial \theta_j} = \sum_k a_{j,k} \hat{U}_{j,k} |\bar{0}\rangle, \quad (11)$$

where

$$\hat{U}_{j,k} = \hat{U}_{N_p} \cdots \hat{U}_{j+1} \hat{U}_j \hat{u}_{j,k} \hat{U}_{j-1} \cdots \hat{U}_1. \quad (12)$$

From Eq. (12), the matrix element $M_{j,k}$ becomes

$$M_{j,k} = \sum_{p,q} \text{Re} \left(a_{j,p}^* a_{k,q} \langle \bar{0} | \hat{U}_{j,p}^\dagger \hat{U}_{j,k} | \bar{0} \rangle \right). \quad (13)$$

For the vector \mathbf{C} , assume the Hamiltonian \hat{H} can be decomposed as $\hat{H} = \sum_j h_j \hat{P}_j$, where h_j is real and \hat{P}_j is a tensor product of Pauli operators. Then,

$$C_j = - \sum_{j,k} \text{Re} \left(a_{j,k} h_j \langle \bar{0} | \hat{U}^\dagger(\boldsymbol{\theta}) \hat{P}_j \hat{U}_{j,k} | \bar{0} \rangle \right). \quad (14)$$

By setting $a_{j,p}^* a_{k,q} = r e^\phi$ ($a_{j,p} = r e^\phi$), each element in $M_{j,k}$ (C_j) can be efficiently calculated by quantum circuits shown in Fig. 1 on the NISQ devices.

The number of circuits required to evaluate M depends on the number of its independent elements. For \mathbf{C} , additional circuits are necessary due to the Hamiltonian decomposition. Since M is a Hermitian ($N_p \times N_p$) matrix and \mathbf{C} is a N_p -dimensional vector, the total number of independent components scales on the order of $\mathcal{O}(N_p^2)$.

III. VARIATIONAL QUANTUM-NEURAL HYBRID EIGEN-SOLVER

In this section, we provide an overview of the Variational Quantum-Neural Hybrid Eigensolver (VQNHE) [29], which combines a parameterized quantum circuit with a neural-network-based post-processing operator to increase the expressive power of variational algorithms for ground-state energy estimation. A key element of VQNHE is the introduction of a non-unitary operator:

$$\hat{f}(\boldsymbol{\phi}) = \sum_{s \in \{0,1\}^{N_q}} f_\phi(s) |s\rangle\langle s|, \quad (15)$$

where $f_\phi(s)$ is a function computed by a NN, $\boldsymbol{\phi}$ is the parameter set of the NN, and s represents a bitstring, and $f_\phi(s)$ is a real-valued function for simplification, which may be complex in more general formulations.

In the NN, we construct multiple layers: an input layer, hidden layers, and an output layer. Throughout this paper, we assume the NN has N_{layer} layers. The activation vector \mathbf{x}_{j+1} in the $(j+1)$ -th layer is computed as

$$\mathbf{x}_{j+1} = g(W_j \mathbf{x}_j + \mathbf{b}_j) \quad (j = 1, \dots, N_{\text{layer}} - 1) \quad (16)$$

where g is a nonlinear activation function, W_j is a weight matrix, and \mathbf{b}_j is a bias vector. Accordingly, the NN parameters $\boldsymbol{\phi}$ are given by $\{W_j, \mathbf{b}_j\}$.

After preparing a parameterized state $|\varphi(\boldsymbol{\theta})\rangle = \hat{U}(\boldsymbol{\theta}) |\bar{0}\rangle$, we aim to compute the expectation value of $\hat{H} = \sum_j h_j \hat{P}_j$ as

$$\langle \hat{H} \rangle = \sum_j h_j \frac{\langle \varphi(\boldsymbol{\theta}, \boldsymbol{\phi}) | \hat{P}_j | \varphi(\boldsymbol{\theta}, \boldsymbol{\phi}) \rangle}{\langle \varphi(\boldsymbol{\theta}, \boldsymbol{\phi}) | \varphi(\boldsymbol{\theta}, \boldsymbol{\phi}) \rangle}, \quad (17)$$

where $|\varphi(\boldsymbol{\theta}, \boldsymbol{\phi})\rangle = \hat{f}(\boldsymbol{\phi}) |\varphi(\boldsymbol{\theta})\rangle$.

In the case of \hat{P}_j that involves only the Pauli \hat{Z} operators, both the numerator and the denominator in Eq. (17) can be efficiently determined by measuring all the qubits along the z axis. The measurement results, represented as bitstrings s , are then fed into the NN to evaluate $f_\phi(s)$.

Let us consider that \hat{P}_j contains the Pauli \hat{X} or \hat{Y} operators. For ease of discussion, we redefine one of the qubits corresponding to \hat{X} or \hat{Y} as the zeroth qubit. The action of \hat{P}_j on $|s\rangle$ is given by $\hat{P}_j |s\rangle = S(\tilde{s}) |\tilde{s}\rangle$, where $S(\tilde{s})$ is a phase factor (± 1) or ($\pm i$), and \tilde{s} represents the transformed bitstring. For example, if $\hat{P}_j = \hat{X}_0 \hat{Y}_1 \hat{Z}_2$ and the bitstring $s = 011$, then $\tilde{s} = 101$. Thus, \hat{P}_j can be expressed as:

$$\hat{P}_j = \sum_{\substack{s_0=0, \\ s_{1:N_q-1} \in \{0,1\}^{N_q-1}}} \left(S(s) |s\rangle\langle \tilde{s}| + S(\tilde{s}) |\tilde{s}\rangle\langle s| \right), \quad (18)$$

where $s_{1:N_q-1}$ represents the subset of s excluding s_0 . Here, $|s\rangle$ can be written as $|s\rangle = |s_0\rangle |s_{1:N_q-1}\rangle$. The eigenstates of \hat{P}_j , which diagonalize \hat{P}_j with eigenvalues ± 1 , are given by:

$$|+, s_{1:N_q-1}\rangle = \frac{1}{\sqrt{2}} \left[S(0s_{1:N_q-1}) |0s_{1:N_q-1}\rangle + |1\tilde{s}_{1:N_q-1}\rangle \right], \quad (19)$$

$$|-, s_{1:N_q-1}\rangle = \frac{1}{\sqrt{2}} \left[S(0s_{1:N_q-1}) |0s_{1:N_q-1}\rangle - |1\tilde{s}_{1:N_q-1}\rangle \right], \quad (20)$$

where we define $|0s_{1:N_q-1}\rangle = |s_0 = 0\rangle |s_{1:N_q-1}\rangle$ and $|1s_{1:N_q-1}\rangle = |s_0 = 1\rangle |s_{1:N_q-1}\rangle$. Hence, the matrix element $\langle \varphi(\boldsymbol{\theta}, \boldsymbol{\phi}) | \hat{P}_j | \varphi(\boldsymbol{\theta}, \boldsymbol{\phi}) \rangle$ can be evaluated as:

$$\begin{aligned} & \langle \varphi(\boldsymbol{\theta}, \boldsymbol{\phi}) | \hat{P}_j | \varphi(\boldsymbol{\theta}, \boldsymbol{\phi}) \rangle \\ &= \sum_{\substack{s_0=0, \\ s_{1:N_q-1} \in \{0,1\}^{N_q-1}}} (|\varphi_{+,s}|^2 - |\varphi_{-,s}|^2) f_\phi(s) f_\phi(\tilde{s}), \end{aligned} \quad (21)$$

where $\varphi_{\pm,s} = \langle \pm, s_{1:N_q-1} | \varphi(\boldsymbol{\theta}) \rangle$. In this approach, the ground-state energy is estimated by optimizing the parameters $\boldsymbol{\theta}$ and $\boldsymbol{\phi}$ by using the gradient method.

We can estimate $|\varphi_{\pm,s}|^2$ using a measurement circuit V designed for the operator \hat{P}_j after implementing $\hat{U}(\boldsymbol{\theta})$. V^\dagger converts $|0s_{1:N_q-1}\rangle$ and $|1s_{1:N_q-1}\rangle$ into $|+, s_{1:N_q-1}\rangle$ and $|-, s_{1:N_q-1}\rangle$ in the absence of a global phase, respectively. For example, when $\hat{P}_j = \hat{X}_0\hat{Y}_1\hat{Z}_2$, the measurement circuit is defined as $H_0\text{CY}_{0,1}$, followed by the measurements on the computational basis, where H_0 denotes the Hadamard gate and $\text{CY}_{0,1}$ denotes the controlled- \hat{Y} gate.

IV. VARIATIONAL QUANTUM-NEURAL HYBRID IMAGINARY TIME EVOLUTION

Here, we propose the hybridization of the VITE algorithm and the NN approach. Before estimating the imaginary-time evolution with our method, we optimize the parameters $\boldsymbol{\theta}$ and $\boldsymbol{\phi}$ for $\beta = \delta\beta$.

A. Preparation of Parameters

When $\beta = 0$, we set $\boldsymbol{\theta} = \mathbf{0}$, $W_{N_{\text{layer}}-1} = 0$, and $b_{N_{\text{layer}}-1} = 0$ since those parameters must satisfy that $\hat{f}_{\boldsymbol{\phi}(\beta=0)}$ and $\hat{U}(\boldsymbol{\theta}(\beta=0))$ are the identity operators. On the other hand, W_k and \mathbf{b}_k ($k = 1, \dots, N_{\text{layer}} - 2$) can take any real values, as they are not constrained by the above condition. Thus, we set those values as random numbers for $\beta = 0$.

If we naively apply the updating rule in Eq. (8) to $\boldsymbol{\theta}(0)$ and $\boldsymbol{\phi}(0)$, we do not always obtain high fidelity during the imaginary-time evolution due to the initial values of W_k and \mathbf{b}_k ($k = 1, \dots, N_{\text{layer}} - 2$). Thus, we next optimize $\boldsymbol{\theta}$ and $\boldsymbol{\phi}$ for $\beta = \delta\beta$. Considering the cost function as $F_{\text{cost}} = 1 - |\langle \psi(\delta\beta) | \tilde{\varphi}(\boldsymbol{\theta}, \boldsymbol{\phi}) \rangle|^2$ where $|\tilde{\varphi}(\boldsymbol{\theta}, \boldsymbol{\phi})\rangle = C(\boldsymbol{\theta}, \boldsymbol{\phi}) |\varphi(\boldsymbol{\theta}, \boldsymbol{\phi})\rangle$ and $C(\boldsymbol{\theta}, \boldsymbol{\phi}) = 1/\sqrt{\langle \varphi(\boldsymbol{\theta}, \boldsymbol{\phi}) | \varphi(\boldsymbol{\theta}, \boldsymbol{\phi}) \rangle}$, the derivatives of F_{cost} are written as

$$\begin{aligned} \frac{\partial F_{\text{cost}}}{\partial \phi_j} &= -2C(\boldsymbol{\theta}, \boldsymbol{\phi}) \left(\frac{\partial C}{\partial \phi_j} |\langle \psi(\delta\beta) | \varphi(\boldsymbol{\theta}, \boldsymbol{\phi}) \rangle|^2 + \right. \\ &C(\boldsymbol{\theta}, \boldsymbol{\phi}) \text{Re} \left(\langle \psi(\delta\beta) | \varphi(\boldsymbol{\theta}, \boldsymbol{\phi}) \rangle \frac{\partial}{\partial \phi_j} \langle \varphi(\boldsymbol{\theta}, \boldsymbol{\phi}) | \psi(\delta\beta) \rangle \right) \left. \right), \end{aligned} \quad (22)$$

$$\begin{aligned} \frac{\partial F_{\text{cost}}}{\partial \theta_j} &= -2C(\boldsymbol{\theta}, \boldsymbol{\phi}) \left(\frac{\partial C}{\partial \theta_j} |\langle \psi(\delta\beta) | \varphi(\boldsymbol{\theta}, \boldsymbol{\phi}) \rangle|^2 + \right. \\ &C(\boldsymbol{\theta}, \boldsymbol{\phi}) \text{Re} \left(\langle \psi(\delta\beta) | \varphi(\boldsymbol{\theta}, \boldsymbol{\phi}) \rangle \frac{\partial}{\partial \theta_j} \langle \varphi(\boldsymbol{\theta}, \boldsymbol{\phi}) | \psi(\delta\beta) \rangle \right) \left. \right). \end{aligned} \quad (23)$$

Here, $\partial_{\phi_j} C = -C^3 D_{\phi_j}$ and $\partial_{\theta_j} C = -C^3 D_{\theta_j}$ appear where

$$D_{\phi_j} = \text{Re} \left(\sum_{s \in \{0,1\}^{N_q}} f_{\boldsymbol{\phi}}(s) \partial_{\phi_j} f_{\boldsymbol{\phi}}(s) |\langle \varphi(\boldsymbol{\theta}) | s \rangle|^2 \right), \quad (24)$$

$$D_{\theta_j} = \text{Re} \left(\sum_{s \in \{0,1\}^{N_q}} f_{\boldsymbol{\phi}}^2(s) \langle \bar{0} | \partial_{\theta_j} \hat{U}^\dagger | s \rangle \langle s | \varphi(\boldsymbol{\theta}) \rangle \right). \quad (25)$$

All the components of $\partial_{\phi_j} F_{\text{cost}}$, $\partial_{\theta_j} F_{\text{cost}}$, D_{ϕ_j} , and D_{θ_j} can be computed with quantum devices as shown in Appendix A. After we update all the parameters as $\phi_j \leftarrow \phi_j - \eta \partial_{\phi_j} F_{\text{cost}}$ and $\theta_j \leftarrow \theta_j - \eta \partial_{\theta_j} F_{\text{cost}}$ the desired number of times, we adopt these updated parameters as $\boldsymbol{\phi}(\beta = \delta\beta)$ and $\boldsymbol{\theta}(\beta = \delta\beta)$.

B. Updating parameters

Here, we propose a hybrid method of the variational quantum circuit and NN for ITE. For approximating Eq. (2) with $|\tilde{\varphi}(\boldsymbol{\theta}, \boldsymbol{\phi})\rangle$, we replace $\boldsymbol{\theta}$ with $\{\boldsymbol{\theta}, \boldsymbol{\phi}\}$ in Eq. (8). Then, the elements of M and C are written with:

$$\begin{aligned} &\text{Re} (\langle \partial_{\phi_j} \tilde{\varphi}(\boldsymbol{\theta}, \boldsymbol{\phi}) | \partial_{\phi_k} \tilde{\varphi}(\boldsymbol{\theta}, \boldsymbol{\phi}) \rangle) \\ &= \text{Re} \left(C^2 \sum_s [\partial_{\phi_j} f_{\boldsymbol{\phi}}^*(s)] [\partial_{\phi_k} f_{\boldsymbol{\phi}}(s)] |\langle \varphi(\boldsymbol{\theta}) | s \rangle|^2 \right. \\ &- C^4 \sum_s \{ D_{\phi_j} f_{\boldsymbol{\phi}}^*(s) [\partial_{\phi_k} f_{\boldsymbol{\phi}}(s)] \\ &+ D_{\phi_k} [\partial_{\phi_j} f_{\boldsymbol{\phi}}^*(s)] f_{\boldsymbol{\phi}}(s) \} |\langle \varphi(\boldsymbol{\theta}) | s \rangle|^2 \\ &\left. + C^4 D_{\phi_j} D_{\phi_k} \right), \end{aligned} \quad (26)$$

$$\begin{aligned} &\text{Re} (\langle \partial_{\theta_j} \tilde{\varphi}(\boldsymbol{\theta}, \boldsymbol{\phi}) | \partial_{\theta_k} \tilde{\varphi}(\boldsymbol{\theta}, \boldsymbol{\phi}) \rangle) \\ &= \left(C^2 \langle \bar{0} | [\partial_{\theta_j} \hat{U}^\dagger] \hat{f}^\dagger(\phi) [\partial_{\theta_k} \hat{f}(\phi)] | \varphi(\boldsymbol{\theta}) \rangle \right. \\ &- C^4 \sum_s \{ D_{\theta_j} [\partial_{\theta_k} f_{\boldsymbol{\phi}}(s)] f_{\boldsymbol{\phi}}^*(s) |\langle \varphi(\boldsymbol{\theta}) | s \rangle|^2 \\ &+ D_{\theta_k} \langle \bar{0} | [\partial_{\theta_j} \hat{U}^\dagger] \hat{f}^\dagger_\phi(s) \} \\ &\left. + C^4 D_{\theta_j} D_{\theta_k} \right), \end{aligned} \quad (27)$$

$$\begin{aligned} &\text{Re} (\langle \partial_{\theta_j} \tilde{\varphi}(\boldsymbol{\theta}, \boldsymbol{\phi}) | \partial_{\theta_k} \tilde{\varphi}(\boldsymbol{\theta}, \boldsymbol{\phi}) \rangle) \\ &= \left(C^2 \langle \bar{0} | [\partial_{\theta_j} \hat{U}^\dagger] \hat{f}^\dagger(\phi) \hat{f}(\phi) [\partial_{\theta_k} \hat{U}] | \bar{0} \rangle \right. \\ &- C^4 \{ D_{\theta_j} \langle \varphi(\boldsymbol{\theta}, \boldsymbol{\phi}) | \hat{f}(\phi) [\partial_{\theta_k} \hat{U}^\dagger] | \bar{0} \rangle \\ &+ D_{\theta_k} \langle \bar{0} | [\partial_{\theta_j} \hat{U}^\dagger] \hat{f}^\dagger(\phi) | \varphi(\boldsymbol{\theta}, \boldsymbol{\phi}) \rangle \} \\ &\left. + C^4 D_{\theta_j} D_{\theta_k} \right), \end{aligned} \quad (28)$$

$$\begin{aligned} & \text{Re} \left(\langle \partial_{\phi_j} \tilde{\varphi}(\boldsymbol{\theta}, \phi) | \hat{H} | \tilde{\varphi}(\boldsymbol{\theta}, \phi) \rangle \right) = \\ & \text{Re} \left(-C^2 D_{\phi_j} E + C \langle \varphi(\boldsymbol{\theta}) | [\partial_{\phi_j} \hat{f}^\dagger(\phi)] \hat{H} | \tilde{\varphi} \rangle \right), \quad (29) \end{aligned}$$

$$\begin{aligned} & \text{Re} \left(\langle \partial_{\theta_j} \tilde{\varphi}(\boldsymbol{\theta}, \phi) | \hat{H} | \tilde{\varphi}(\boldsymbol{\theta}, \phi) \rangle \right) = \\ & \text{Re} \left(-C^2 D_{\theta_j} E + C \langle \bar{0} | [\partial_{\theta_j} \hat{U}^\dagger] \hat{f}^\dagger(\phi) \hat{H} | \tilde{\varphi} \rangle \right), \quad (30) \end{aligned}$$

where we define $E \equiv \langle \tilde{\varphi} | \hat{H} | \tilde{\varphi} \rangle$.

We can obtain $\langle \bar{0} | [\partial_{\theta_j} \hat{U}^\dagger] \hat{f}^\dagger(\phi) [\partial_{\phi_k} \hat{f}(\phi)] | \varphi(\boldsymbol{\theta}) \rangle$ in Eq. (27), $\langle \bar{0} | [\partial_{\theta_j} \hat{U}^\dagger] \hat{f}^\dagger(\phi) \hat{f}(\phi) [\partial_{\theta_k} \hat{U}] | \bar{0} \rangle$ in Eq. (28), $\langle \varphi(\boldsymbol{\theta}) | [\partial_{\phi_j} \hat{f}^\dagger(\phi)] \hat{H} | \tilde{\varphi} \rangle$ in Eq. (29), and $\langle \bar{0} | [\partial_{\theta_j} \hat{U}^\dagger] \hat{f}^\dagger(\phi) \hat{H} | \tilde{\varphi} \rangle$ in Eq. (30) with the Hadamard test as shown in Appendix A. Although it requires more types of quantum circuits to estimate M and C than the conventional scheme, our scheme is still feasible and is expected to achieve higher fidelity with the exact ITE state.

V. NUMERICAL CALCULATION

TABLE I: The value of longitudinal magnetic field strength used in Eq. (31)

h_1	0.9304842831042459
h_2	-0.9766906124157178
h_3	0.4719832395937509
h_4	-0.6839745504705037
h_5	0.9726789033256467
h_6	-0.9662386915840475

In this section, we demonstrate that VQNHTE achieves higher accuracy compared to conventional VITE. As a strict evaluation, we consider the fidelity between the state evolved with the exact ITE and the state obtained with the VQNHTE or VITE method. The initial state is taken as the all-plus state $|+\dots+\rangle$.

In actual devices, interconnectivity is limited. Thus, we consider two types of quantum circuits: the circuit in Fig. 2(a) includes only nearest-neighbor interactions, and the circuit in Fig. 2(b) consists of all-to-all interactions. For the numerical setup, we employed the Heisenberg Hamiltonian with an added longitudinal magnetic field:

$$\begin{aligned} \hat{H} &= \hat{H}_{\text{Heisenberg}} + \hat{H}_{\text{field}} \\ &= J \sum_{j=1}^{N-1} (\hat{\sigma}_j^x \hat{\sigma}_{j+1}^x + \hat{\sigma}_j^y \hat{\sigma}_{j+1}^y + \hat{\sigma}_j^z \hat{\sigma}_{j+1}^z) + \sum_{j=1}^N h_j \hat{\sigma}_j^z, \quad (31) \end{aligned}$$

Here, N denotes the number of qubits, J represents the strength of the exchange interaction, and h_j indicates the strength of the longitudinal magnetic field acting on the j th qubit. In our numerical calculations, we set $N = 6$, $J = -1$, and assigned the values of h_j using random

numbers, with the specific values given in Table. I. For the gradient descent used during the optimization of the initial parameters, we performed 500 iterations with a learning rate of 0.1.

Figure 3 plots the fidelity on the vertical axis and the imaginary time on the horizontal axis. The imaginary time is incremented in steps of 0.1, and the plot shows results from 0.1 to 10. The fidelity calculated using VITE is represented by orange square markers, while the fidelity obtained using VQNHTE is represented by blue markers. Since our method provides the NN with random initial values, the plot shows the average and standard error over 100 samples.

For both sets of validation results, it is clear that VQNHTE estimates the ITE with higher accuracy compared to conventional VITE, and the discrepancy becomes more pronounced as the imaginary time increases.

VI. CONCLUSION

We propose a novel method of ITE, named VQNHTE, which combines VITE with the NN. The VQNHTE algorithm more accurately estimates ITE than conventional VITE by employing the NN to update the parameters of a parametrized circuit, all while operating within the constraints of limited quantum computing resources. The validity of our results was verified through numerical simulations. It should be noted, however, that our method employs a gradient-based approach to properly select the initial parameters for the NN. Adopting this gradient-based method increases the computational time and sampling costs compared to VITE. Nevertheless, we consider that even after taking the added sampling overhead into account, our approach remains practically feasible.

VII. ACKNOWLEDGMENT

This work is supported by JST Moonshot (Grant Number JPMJMS226C).

Appendix A: Quantum circuits for evaluating the derivatives

Here, we show quantum circuits computing derivatives. We can compute D_{ϕ_j} by obtaining $|\langle \varphi(\boldsymbol{\theta}) | s \rangle|^2$ with the measurements on all the qubits in the computational basis and then feeding the measurement result s to $f_\phi(s) [\partial_{\phi_i} f_\phi(s)]$.

Using Eq. (11), D_{θ_j} can be rewritten as

$$D_{\theta_j} = \text{Re} \left(\sum_{s \in \{0,1\}^{N_q}} \sum_k a_{j,k} f_\phi^2(s) \langle \varphi(\boldsymbol{\theta}) | s \rangle \langle s | \hat{U}_{j,k} | \bar{0} \rangle \right). \quad (A1)$$

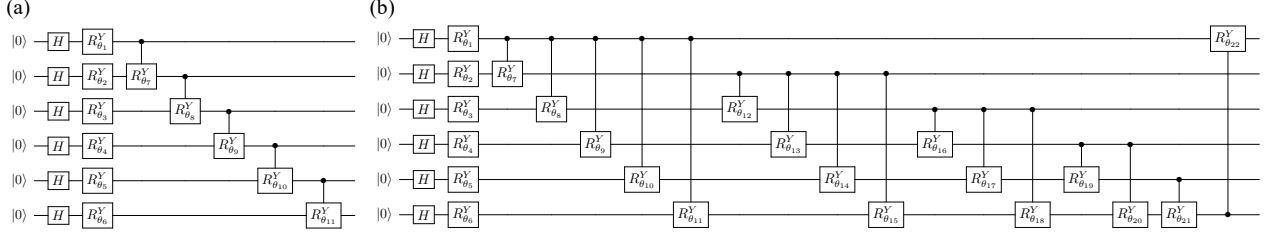


FIG. 2: the ansatz circuit. Here, we consider the case where only single-qubit rotation gates and (a)nearest-neighbor interactions or (b)all-to-all interactions are present. Here, $R_{\theta_i}^Y$ denotes a rotation along the Y-axis, and θ_i represents the parameter of the i th rotation angle.

We define $a_{j,k} = r_{j,k}e^{i\phi_{j,k}}$ where $r_{j,k}$ denotes the amplitude and $\phi_{j,k}$ denotes the phase. We can evaluate the real part of $e^{i\phi_{j,k}} \langle \varphi(\boldsymbol{\theta}) | s \rangle \langle s | \hat{U}_{j,k} | \bar{0} \rangle$ with the circuit described in Fig. 4(a)-1. In this case, we do not operate the measurement circuit V in Fig. 4(a)-1. By inputting the measurement result s into $f_{\phi}^2(s)$ and taking the sum over those terms, we obtain D_{θ_j} . We can also obtain $\text{Re} \left(\langle \bar{0} | [\partial_{\theta_j} \hat{U}^\dagger] \hat{f}^\dagger(\phi) [\partial_{\phi_k} \hat{f}(\phi)] | \varphi(\boldsymbol{\theta}) \rangle \right)$ in Eq. (27) with the circuit in Fig. 4(a)-1 because it is expanded as

$$\begin{aligned} & \text{Re} \left(\langle \varphi(\boldsymbol{\theta}) | [\partial_{\phi_k} \hat{f}^\dagger(\phi)] \hat{f}(\phi) [\partial_{\theta_j} \hat{U}] | \bar{0} \rangle \right) \\ &= \text{Re} \left(\sum_{s \in \{0,1\}^{N_q}} \sum_l a_{j,l} [\partial_{\phi_k} f_{\phi}^*(s)] f_{\phi}(s) \langle \varphi(\boldsymbol{\theta}) | s \rangle \langle s | \hat{U}_{j,l} | \bar{0} \rangle \right). \end{aligned} \quad (\text{A2})$$

$\text{Re} \left(\langle \bar{0} | [\partial_{\theta_j} \hat{U}^\dagger] \hat{f}^\dagger(\phi) \hat{f}(\phi) [\partial_{\theta_k} \hat{U}] | \bar{0} \rangle \right)$ in Eq. (28) is decomposed as

$$\begin{aligned} & \text{Re} \left(\langle \bar{0} | [\partial_{\theta_j} \hat{U}^\dagger] \hat{f}^\dagger(\phi) \hat{f}(\phi) [\partial_{\theta_k} \hat{U}] | \bar{0} \rangle \right) \\ &= \text{Re} \left(\sum_{s \in \{0,1\}^{N_q}} \sum_{l_1} \sum_{l_2} a_{j,l_1}^* a_{k,l_2} f_{\phi}^2 \langle \bar{0} | \hat{U}_{j,l_1}^\dagger | s \rangle \langle s | \hat{U}_{k,l_2} | \bar{0} \rangle \right). \end{aligned} \quad (\text{A3})$$

By defining $a_{j,l_1}^* a_{k,l_2} = r_{j,l_1,k,l_2} e^{i\phi_{j,l_1,k,l_2}}$, we can evaluate $\text{Re} \left(e^{i\phi_{j,l_1,k,l_2}} \langle \bar{0} | \hat{U}_{j,l_1}^\dagger | s \rangle \langle s | \hat{U}_{k,l_2} | \bar{0} \rangle \right)$ with the circuit drawn in Fig. 4 (b).

$\langle \varphi(\boldsymbol{\theta}) | [\partial_{\phi_j} \hat{f}^\dagger(\phi)] \hat{H} | \tilde{\varphi} \rangle$ introduced in Eq. (29) is decomposed as

$$\begin{aligned} & \langle \varphi(\boldsymbol{\theta}) | [\partial_{\phi_j} \hat{f}^\dagger(\phi)] \hat{H} | \tilde{\varphi} \rangle \\ &= C \sum_j h_j \langle \varphi(\boldsymbol{\theta}) | [\partial_{\phi_j} \hat{f}(\phi)] \hat{P}_j \hat{f}(\phi) | \varphi(\boldsymbol{\theta}) \rangle \\ &= C \sum_j \sum_{\substack{s_0=0, \\ s_{1:N_q-1} \in \{0,1\}^{N_q-1}}} h_j (|\varphi_{+,s}|^2 \\ & \quad - |\varphi_{-,s}|^2) [\partial_{\phi_j} f_{\phi}(s)] f_{\phi}(\tilde{s}), \end{aligned} \quad (\text{A4})$$

where we used Eq. (21). Since we can evaluate $|\varphi_{\pm,s}|^2$ with the measurement circuit V as we discussed in Sec. III, we can obtain $\langle \varphi(\boldsymbol{\theta}) | [\partial_{\phi_j} \hat{f}^\dagger(\phi)] \hat{H} | \tilde{\varphi} \rangle$.

We expand $\text{Re} \left(\langle \tilde{\varphi} | \hat{H} \hat{f} \partial_{\theta_i} \hat{U} | \bar{0} \rangle \right)$ introduced in Eq. (30) as

$$\begin{aligned} & \text{Re} \left(\langle \tilde{\varphi} | \hat{H} \hat{f} \partial_{\theta_i} \hat{U} | \bar{0} \rangle \right) \\ &= C(\boldsymbol{\theta}, \phi) \sum_j h_j \text{Re} \left(\langle \varphi(\boldsymbol{\theta}) | \hat{f} \hat{P}_j \hat{f} \partial_{\theta_i} \hat{U} | \bar{0} \rangle \right) \\ &= C(\boldsymbol{\theta}, \phi) \sum_{\substack{j, \\ s_0=0, \\ s_{1:N_q-1} \in \{0,1\}^{N_q-1}}} h_j \text{Re} \left(\varphi_{+,s}^{\theta_i} - \varphi_{-,s}^{\theta_i} \right) f_{\phi}(s) f_{\phi}(\tilde{s}) \\ &= C(\boldsymbol{\theta}, \phi) \sum_{\substack{j,k, \\ s_0=0, \\ s_{1:N_q-1} \in \{0,1\}^{N_q-1}}} h_j \text{Re} \left(a_{k,i} \left(\varphi_{+,s}^{\theta_i,k} - \varphi_{-,s}^{\theta_i,k} \right) \right) f_{\phi}(s) f_{\phi}(\tilde{s}) \end{aligned} \quad (\text{A5})$$

where $\varphi_{\pm,s}^{\theta_i} = \langle \varphi(\boldsymbol{\theta}) | \pm, s_{1:N_q-1} \rangle \langle \pm, s_{1:N_q-1} | \partial_{\theta_i} \varphi(\boldsymbol{\theta}) \rangle$ and $\varphi_{\pm,s}^{\theta_i,k} = \langle \varphi(\boldsymbol{\theta}) | \pm, s_{1:N_q-1} \rangle \langle \pm, s_{1:N_q-1} | \hat{U}_{k,i} | \bar{0} \rangle$. By defining $a_{k,i} = r_{k,i} e^{i\phi_{k,i}}$, we can evaluate $\text{Re} \left(e^{i\phi_{k,i}} \varphi_{\pm,s}^{\theta_i,k} \right)$ with the circuit drawn in Fig. Fig: circuit(a)-2. In this case, the measurement circuit V is implemented.

Next, let us consider $\langle \psi(\delta\beta) | \varphi(\boldsymbol{\theta}, \phi) \rangle$ appearing in Eqs. (22) and (23). If $\delta\beta$ is sufficiently small, the imaginary-time operator is approximated as

$$\begin{aligned} \exp(-\hat{H}\delta\beta) &\simeq I - \hat{H}\delta\beta + \frac{1}{2}(\hat{H}\delta\beta)^2 \\ &= \sum_i e_i \hat{P}_i, \end{aligned} \quad (\text{A6})$$

where e_i is a coefficient and \hat{P}_i is a tensor product of Pauli matrices. Here, we ignore the third and higher-order terms. We can aim for more precision by increasing the truncation order although it takes more computational costs. Thus, $\langle \psi(\delta\beta) | \varphi(\boldsymbol{\theta}, \phi) \rangle$ is expanded as

$$\begin{aligned} & \langle \psi(\delta\beta) | \varphi(\boldsymbol{\theta}, \phi) \rangle \\ &= \sum_{s \in \{0,1\}^{N_q}} \sum_i e_i f_{\phi}(s) \langle \bar{0} | \hat{P}_i | s \rangle \langle s | U(\boldsymbol{\theta}) | \bar{0} \rangle, \end{aligned} \quad (\text{A7})$$

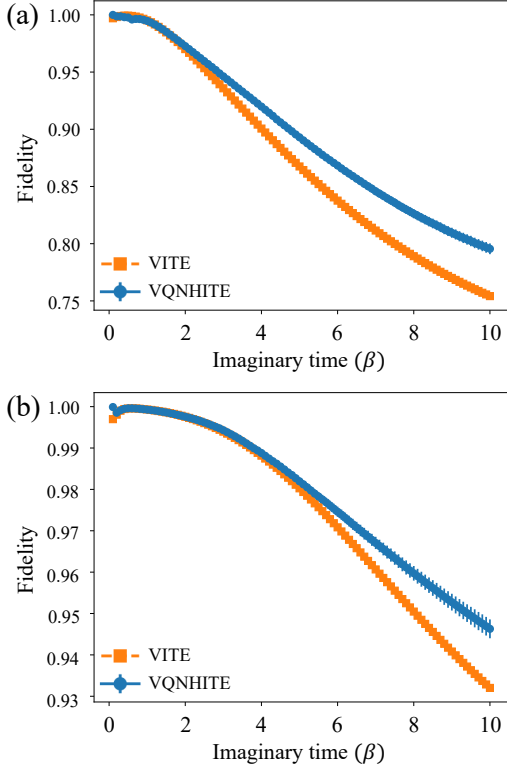


FIG. 3: We plot the fidelity (vertical axis) between the states obtained via VQNHTE (blue markers) or VITE (orange square markers) and the exact imaginary time-evolved state, as a function of imaginary time (horizontal axis), incremented in steps of 0.1 from 0.1 to 10. (a) Results using the ansatz circuit that accounts only for nearest-neighbor interactions, as shown in Fig.2(a). (b) Results using the ansatz circuit that includes all-to-all interactions, shown in Fig.2(b). In our numerical calculations, we set $N = 6$, $J = -1$ and assigned the values of h_j randomly, with the specific values given in Table I.

where the real and imaginary parts of $\langle \psi(0) | \hat{P}_i | s \rangle \langle s | \varphi(\theta) \rangle$ are computed with the circuit described in Fig. 4 (c). Because $\partial_{\phi_k} \langle \psi(\delta\beta) | \varphi(\theta, \phi) \rangle$ is decomposed as

$$\begin{aligned} & \partial_{\phi_k} \langle \psi(\delta\beta) | \varphi(\theta, \phi) \rangle \\ = & \sum_{s \in \{0,1\}^{N_q}} \sum_i e_i \partial_{\phi_k} f_{\phi}(s) \langle \bar{0} | \hat{P}_i | s \rangle \langle s | U(\theta) | \bar{0} \rangle, \end{aligned} \quad (\text{A8})$$

the real and imaginary parts of this term are also computed with the circuit in Fig. 4 (c).

Finally, let us consider $\partial\theta_k \langle \psi(\delta\beta) | \varphi(\theta, \phi) \rangle$. This term

is decomposed as

$$\begin{aligned} & \partial\theta_k \langle \psi(\delta\beta) | \varphi(\theta, \phi) \rangle \\ = & \sum_{s \in \{0,1\}^{N_q}} \sum_{i,j} e_i f_{\phi}(s) r_{k,i} e^{i\phi_{k,i}} \langle \bar{0} | \hat{P}_i | s \rangle \langle s | \hat{U}_{k,j} | \bar{0} \rangle. \end{aligned} \quad (\text{A9})$$

Because we can compute the real and imaginary parts of $e^{i\phi_{k,i}} \langle \bar{0} | \hat{P}_i | s \rangle \langle s | \hat{U}_{k,j} | \bar{0} \rangle$ with the circuit in Fig. 4 (d), $\partial\theta_k \langle \psi(\delta\beta) | \varphi(\theta, \phi) \rangle$ can also be computed.

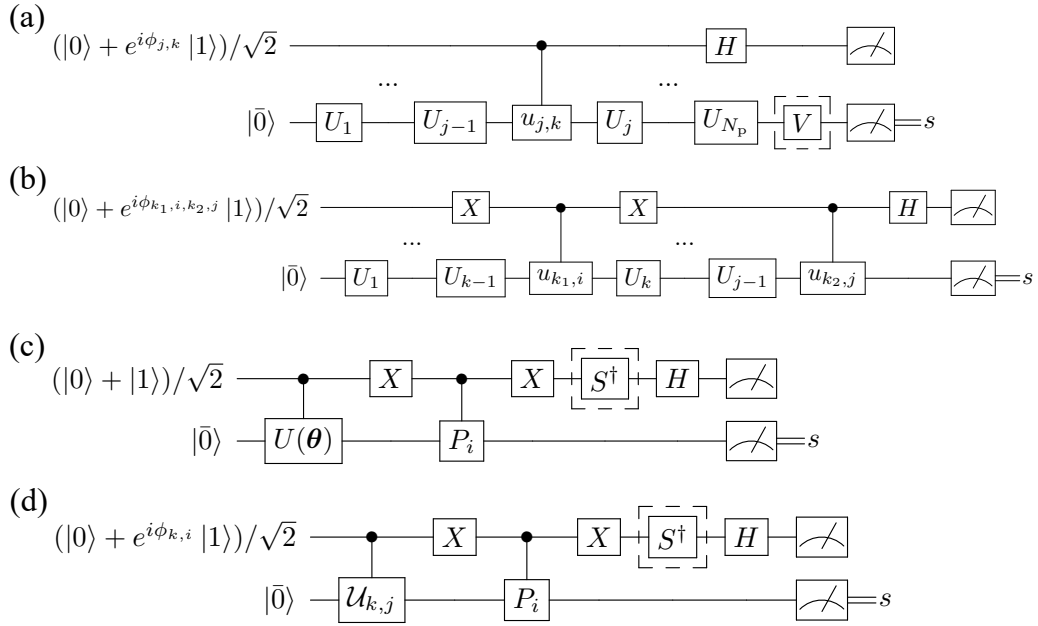


FIG. 4: Quantum circuits for calculating (a)-1 $e^{i\phi_{j,k}} \langle \varphi(\theta) | s \rangle \langle s | \hat{U}_{j,k} | \bar{0} \rangle$. In this case, we do not operate the measurement circuit V . (a)-2 $\text{Re} \left(\langle \bar{0} | [\partial_{\theta_j} \hat{U}^\dagger] \hat{f}^\dagger(\phi) [\partial_{\phi_k} \hat{f}(\phi)] | \varphi(\theta) \rangle \right)$. In this case, measurement circuit V is implemented. (b) $\text{Re} \left(e^{i\phi_{j, l_1, k, l_2}} \langle \bar{0} | \hat{U}_{j, l_1}^\dagger | s \rangle \langle s | \hat{U}_{k, l_2} | \bar{0} \rangle \right)$, (c) $\langle \psi(\delta\beta) | \varphi(\theta, \phi) \rangle$, and $\partial \theta_k \langle \psi(\delta\beta) | \varphi(\theta, \phi) \rangle$. The upper horizontal line (the lower line) represents the ancillary qubit (the qubits of the system).

-
- [1] S.-H. Lin, R. Dilip, A. G. Green, A. Smith, and F. Pollmann, *PRX Quantum* **2**, 010342 (2021).
- [2] N. Schuch, M. M. Wolf, F. Verstraete, and J. I. Cirac, *Physical review letters* **98**, 140506 (2007).
- [3] S. McArdle, T. Jones, S. Endo, Y. Li, S. C. Benjamin, and X. Yuan, *npj Quantum Information* **5**, 75 (2019).
- [4] A. A. Houck, H. E. Türeci, and J. Koch, *Nature Physics* **8**, 292 (2012).
- [5] T. Horikiri, M. Yamaguchi, K. Kamide, Y. Matsuo, T. Byrnes, N. Ishida, A. Löffler, S. Höfling, Y. Shikano, T. Ogawa, et al., *Scientific reports* **6**, 25655 (2016).
- [6] P. J. O'Malley, R. Babbush, I. D. Kivlichan, J. Romero, J. R. McClean, R. Barends, J. Kelly, P. Roushan, A. Tranter, N. Ding, et al., *Physical Review X* **6**, 031007 (2016).
- [7] R. Gerritsma, G. Kirchmair, F. Zähringer, E. Solano, R. Blatt, and C. Roos, *Nature* **463**, 68 (2010).
- [8] J. I. Cirac and P. Zoller, *Nature physics* **8**, 264 (2012).
- [9] I. M. Georgescu, S. Ashhab, and F. Nori, *Reviews of Modern Physics* **86**, 153 (2014).
- [10] T. Byrnes, P. Recher, and Y. Yamamoto, *Physical Review B—Condensed Matter and Materials Physics* **81**, 205312 (2010).
- [11] I. Buluta and F. Nori, *Science* **326**, 108 (2009).
- [12] W. M. Foulkes, L. Mitas, R. Needs, and G. Rajagopal, *Reviews of Modern Physics* **73**, 33 (2001).
- [13] T. Jones, S. Endo, S. McArdle, X. Yuan, and S. C. Benjamin, *Physical Review A* **99**, 062304 (2019).
- [14] J. Gacon, J. Nys, R. Rossi, S. Woerner, and G. Carleo, *Physical Review Research* **6**, 013143 (2024).
- [15] K. Yeter-Aydeniz, E. Moschandreou, and G. Siopsis, *Physical Review A* **105**, 012412 (2022).
- [16] K. Yeter-Aydeniz, G. Siopsis, and R. C. Pooser, *New Journal of Physics* **23**, 043033 (2021).
- [17] S.-N. Sun, M. Motta, R. N. Tazhigulov, A. T. Tan, G. K.-L. Chan, and A. J. Minnich, *PRX Quantum* **2**, 010317 (2021).
- [18] K. Yeter-Aydeniz, R. C. Pooser, and G. Siopsis, *npj Quantum Information* **6**, 63 (2020).
- [19] T. Liu, J.-G. Liu, and H. Fan, *Quantum Information Processing* **20**, 204 (2021).
- [20] J. Preskill, *Bulletin of the American Physical Society* **64**, 9 (2019).
- [21] A. Peruzzo, J. McClean, P. Shadbolt, M.-H. Yung, X.-Q. Zhou, P. J. Love, A. Aspuru-Guzik, and J. L. O'Brien, *Nature communications* **5**, 4213 (2014).
- [22] J. R. McClean, J. Romero, R. Babbush, and A. Aspuru-Guzik, *New Journal of Physics* **18**, 023023 (2016).
- [23] C. Hempel, C. Maier, J. Romero, J. McClean, T. Monz, H. Shen, P. Jurcevic, B. P. Lanyon, P. Love, R. Babbush, et al., *Physical Review X* **8**, 031022 (2018).
- [24] J.-G. Liu, Y.-H. Zhang, Y. Wan, and L. Wang, *Physical Review Research* **1**, 023025 (2019).
- [25] Y. Cao, J. Romero, J. P. Olson, M. Degroote, P. D. Johnson, M. Kieferová, I. D. Kivlichan, T. Menke, B. Peropadre, N. P. Sawaya, et al., *Chemical reviews* **119**, 10856 (2019).
- [26] S. McArdle, S. Endo, A. Aspuru-Guzik, S. C. Benjamin, and X. Yuan, *Reviews of Modern Physics* **92**, 015003 (2020).
- [27] B. Bauer, S. Bravyi, M. Motta, and G. K.-L. Chan, *Chemical reviews* **120**, 12685 (2020).
- [28] D. Amaro, C. Modica, M. Rosenkranz, M. Fiorentini, M. Benedetti, and M. Lubasch, *Quantum Science and Technology* **7**, 015021 (2022).
- [29] S.-X. Zhang, Z.-Q. Wan, C.-K. Lee, C.-Y. Hsieh, S. Zhang, and H. Yao, *Physical Review Letters* **128**, 120502 (2022).
- [30] J.-G. Liu and L. Wang, *Physical Review A* **98**, 062324 (2018).
- [31] J.-G. Liu, L. Mao, P. Zhang, and L. Wang, *Machine Learning: Science and Technology* **2**, 025011 (2021).
- [32] G. Verdon, J. Marks, S. Nanda, S. Leichenauer, and J. Hidary, *arXiv preprint arXiv:1910.02071* (2019).
- [33] C. Y. Hsieh, Q. Sun, S. Zhang, and C. K. Lee, *npj Quantum Information* **7**, 19 (2021).
- [34] M. Benedetti, B. Coyle, M. Fiorentini, M. Lubasch, and M. Rosenkranz, *Physical Review Applied* **16**, 044057 (2021).
- [35] J. Rivera-Dean, P. Huembeli, A. Acín, and J. Bowles, *arXiv preprint arXiv:2104.02955* (2021).
- [36] G. Torlai, G. Mazzola, G. Carleo, and A. Mezzacapo, *Physical Review Research* **2**, 022060 (2020).
- [37] E. R. Bennewitz, F. Hopfmueller, B. Kulchitsky, J. Carrasquilla, and P. Ronagh, *Nature Machine Intelligence* **4**, 618 (2022).
- [38] A. Sagingalieva, M. Kordzanganeh, A. Kurkin, A. Melnikov, D. Kuhmistrov, M. Perelshtein, A. Melnikov, A. Skolik, and D. V. Dollen, *Quantum Machine Intelligence* **5**, 38 (2023).
- [39] S. Liu, S.-X. Zhang, S.-K. Jian, and H. Yao, *Physical Review Research* **5**, L032040 (2023).
- [40] A. Sagingalieva, A. Kurkin, A. Melnikov, D. Kuhmistrov, M. Perelshtein, A. Melnikov, A. Skolik, and D. Von Dollen, *arXiv preprint arXiv:2205.04878* (2022).
- [41] J. Miao, C.-Y. Hsieh, and S.-X. Zhang, *Physical Review Applied* **21**, 014053 (2024).
- [42] G. C. Wick, *Phys. Rev.* **96**, 1124 (1954).
- [43] M. E. Peskin, *An Introduction to quantum field theory* (CRC press, 2018).
- [44] M. Motta, C. Sun, A. T. Tan, M. J. O'rourke, E. Ye, A. J. Minnich, F. G. Brandao, and G. K.-L. Chan, *arXiv preprint arXiv:1901.07653* **10** (2019).
- [45] H.-L. Huang, X.-Y. Xu, C. Guo, G. Tian, S.-J. Wei, X. Sun, W.-S. Bao, and G.-L. Long, *Science China Physics, Mechanics & Astronomy* **66**, 250302 (2023).